

Biochemical adaptations of the retina and retinal pigment epithelium support a metabolic ecosystem in the vertebrate eye

Mark A. Kanow¹, Michelle M. Giarmarco¹, Connor Jankowski¹, Kristine Tsantilas¹, Abbi L. Engel¹, Jianhai Du^{4,5}, Jonathan D. Linton^{1,2}, Christopher C. Farnsworth¹, Stephanie R. Sloat¹, Ken J. Lindsay^{1,5}, Edward D. Parker², Susan E. Brockerhoff^{1,2}, Martin Sadilek³, Jennifer R. Chao² and James B. Hurley^{1,2,6}

¹Dept. of Biochemistry, ²Dept. of Ophthalmology, ³Dept. of Chemistry, University of Washington, Seattle, WA 98195

⁴Dept. of Ophthalmology, ⁵Dept. of Biochemistry, West Virginia University, One Medical Center Drive, PO Box 9193, Morgantown, WV 26506

⁵Fred Hutchinson Cancer Research Center, Seattle, WA 98109

⁶Lead contact

Correspondence: jbhhh@uw.edu

1 **ABSTRACT**

2 Here we report multiple lines of evidence for a comprehensive model for retinal
3 energy metabolism. Metabolic flux, locations of key enzymes and our finding that
4 glucose enters the neural retina almost entirely through photoreceptors support a
5 conceptually new model for retinal metabolism. In this model, glucose from the
6 choroidal blood supply passes through the retinal pigment epithelium to the retina
7 where photoreceptors convert it to lactate. Photoreceptors then export the lactate
8 as fuel for the retinal pigment epithelium and for neighboring Müller glial cells. A
9 key feature of this model is that aerobic glycolysis in photoreceptors produces
10 lactate to suppress glycolysis in the neighboring retinal pigment epithelium. That
11 enhances the flow of glucose to the retina by minimizing consumption of glucose
12 within the retinal pigment epithelium. This framework for metabolic relationships
13 in retina provides new insights into the underlying causes of retinal disease, age-
14 related vision loss and metabolism-based therapies.

15

16 INTRODUCTION

17 Mutations in any of more than 140 genes can cause photoreceptors in a
18 vertebrate retina to degenerate (1). The relationship between photoreceptor
19 degeneration and the diversity of biochemical functions and expression patterns
20 of those genes is enigmatic. The diversity suggests that the consequences of
21 loss or gain of function of these genes may converge onto a few essential
22 metabolic processes (2, 3). Much has been gained by studying specific functions
23 of the genes. Based on those studies therapeutic strategies for specific genetic
24 deficiencies are being developed (4). Nevertheless, a more general approach to
25 understanding what photoreceptors need to survive could lead to more broadly
26 applicable therapeutic strategies. With that in mind, we have been investigating
27 the fundamental nature of energy metabolism in the retina and the retinal
28 pigment epithelium (RPE) (5-11).

29 Glucose that fuels the outer retina comes from the choroidal blood. Before it can
30 reach the retina, however, the glucose first must traverse the RPE. The RPE is a
31 monolayer of polarized cells between the choroid and retina that functions as a
32 blood-retina barrier. The cells in the RPE are bound together by tight junctions
33 and they express specific transporter proteins on their basolateral and apical
34 surfaces (12). Glucose from the choroid passes through transporters on the
35 basolateral surface, and then wends its way through the cytoplasm of the RPE
36 cell. If metabolic enzymes within the RPE cell do not consume it, glucose moves
37 down a concentration gradient toward the opposite side of the RPE cell where it
38 exits to the retina through transporters on the apical surface of the RPE.

39 When the glucose reaches the retina most of it is consumed by glycolysis and
40 converted to lactate. Retinas and tumors were the two tissues first identified in
41 the 1920's by Warburg (13) as relying mostly on "aerobic glycolysis". This type of
42 metabolism can release massive amounts of lactate from a cell even when O₂ is
43 available. Evidence indicates that photoreceptors in the outer retina are the site
44 of aerobic glycolysis (8, 13-17). The importance of aerobic glycolysis for survival
45 and function of photoreceptors has not been established, but it is thought to
46 enhance anabolic activity within the photoreceptor (3, 18-20).

47 In RPE cells energy metabolism is strikingly different than in the retina. In
48 particular, RPE cells are specialized for a type of energy metabolism called
49 reductive carboxylation (9) that aids in redox homeostasis. In general, RPE cells
50 rely more on their mitochondria.

51 Recent reports described genetic manipulations that explored the effects of
52 qualitatively altering energy metabolism either in photoreceptors or in RPE cells
53 *in vivo*. Glycolysis in rods was enhanced in one study by blocking expression of
54 SIRT6 (3). Another study enhanced glycolysis in rods by activating mTORC1 (21).
55 Those studies showed that making photoreceptors more glycolytic makes them
56 more robust. Both strategies slowed degeneration of rods caused by mutations
57 associated with retinitis pigmentosa (3, 21). However, making RPE cells more
58 glycolytic *in vivo* has the opposite effect; it causes neighboring photoreceptors to
59 degenerate. When glycolysis in the RPE was enhanced by knocking out VHL

60 (22) or by knocking out an essential mitochondrial transcription factor in RPE
61 cells *in vivo* (23) the neighboring photoreceptors died.

62 The findings of those *in vivo* studies appear puzzling and seemingly contradictory
63 when considered only from a cell autonomous perspective. Why does enhancing
64 glycolysis help some cells and endanger others? Here we propose that those
65 findings make more sense when interpreted in the context of metabolic
66 relationships between the retina and the RPE. We describe evidence that the
67 retina and RPE function as a metabolic ecosystem. We show that photoreceptors
68 are the main point of entry for glucose into the retina. The photoreceptors convert
69 glucose to lactate, which then serves as a fuel for other cells in the retina. We
70 show here that lactate also can enhance the ability of RPE cells to pass glucose
71 from the blood to the retina. The model that we propose based on these findings
72 predicts that each cell in the retina and RPE contributes an essential metabolic
73 function that promotes survival of the complete retina-RPE ecosystem.

74

75 **RESULTS**

76 **Photoreceptors express a glucose transporter.** Uptake of glucose into cells
77 requires a protein that can transport glucose. We used immunoblotting of mouse
78 tissues to evaluate expression of glucose transporters (**Fig. 1A**) and confirmed
79 previous findings that GLUT1 is the primary glucose transporter isoform in retina
80 (24) and RPE (25). The protein immunoreactive with the GLUT1 antibody was
81 confirmed to be membrane associated (**Fig. 1B**). GLUT3 was detected only in
82 brain. GLUT4 was detected in heart and muscle as expected, but not in the retina.

83 Immunohistochemistry shows that GLUT1 immunoreactivity overlaps with
84 cytochrome oxidase subunit 1 (MT-CO1) (**Fig. 1C**), which identifies rod inner
85 segments by the unique elongated shape of their mitochondria (**Fig 1E**). These
86 mitochondria extend beyond the ends of the Müller glial cell (MGC) apical
87 processes (**Fig 1E**). There are no mitochondria within these fine MGC apical
88 processes. Instead, small spherical-shaped mitochondria line up within the
89 MGCs along the outer limiting membrane just beneath the apical processes (**Fig.**
90 **1F and arrowheads in Fig. 1C**). MGCs extend from the outer limiting membrane
91 to the ganglion cell side of the retina. Most of the GLUT1 immunoreactivity in
92 MGCs is in the inner retina (**Fig. 1D**). GLUT1 immunoreactivity also overlaps with
93 a marker specific for rod photoreceptors, rod arrestin (**Fig. 1G**) and it overlaps
94 with GFP expressed from the rod-specific *Nrl* promoter (**Fig. 1H**). Taken
95 altogether, the distribution of GLUT1 immunoreactivity supports the idea that
96 photoreceptors can take up glucose released from the apical side of the RPE.

97 **Dietary glucose enters the retina primarily through photoreceptors.** Next we
98 asked which cells in the retina take up glucose in the context of an eye within a
99 living animal. We used oral gavage to introduce a fluorescent derivative of 2-
100 deoxy glucose (2-NBDG) (26) into stomachs of mice. We harvested the retinas
101 20 or 60 minutes after gavage, mounted them on filter paper and cut slices for
102 imaging by confocal microscopy (27). **Fig. 2A** shows that 2-NBDG fluorescence
103 is strongest in the photoreceptor layer, suggesting that photoreceptors are the

104 first cells in the retina to take up glucose from the blood. Surprisingly, 2-NBDG
105 fluorescence is stronger in the outer retina than in the inner retina even though
106 mouse inner retinas are vascularized. We noted that 2-NBDG fluorescence does
107 not overlap with Müller Glial Cells (MGC's), which were labeled in these
108 experiments by transgenic expression of tdTomato (28), though in rare instances
109 there was overlap at a MGC end foot.. These results are summarized and
110 quantified in **Fig. 2C**. They show that glucose that reaches the outer retina is
111 taken up primarily by photoreceptors and not MGC's.

112 The images in **Fig. 2A** were made from live, unfixed mouse retinas. Most
113 photoreceptors in mouse retinas are rods. It is difficult in these images to resolve
114 whether cones also import 2-NBDG. To address this we also introduced 2-NBDG
115 by oral gavage into adult zebrafish, whose retinas are more enriched with cones
116 (29). **Fig. 2B** shows that cones become intensely fluorescent 30 minutes after
117 gavage. As in mouse retinas, there was no indication of glucose uptake into
118 MGCs, which in these retinas were marked with tdTomato expressed from a
119 GFAP promoter (30). **Fig. 2D** reports quantification and summarizes the
120 zebrafish retina results.

121 **Carbons from glucose are metabolized in RPE cells more slowly than in**
122 **retina.** Previous studies showed that most of the glucose taken up into a retina is
123 used to make lactic acid (8, 13-17). Within the eye of a living animal, glucose
124 from the choroidal blood first must pass through the monolayer of RPE cells
125 before it can reach the retina. We hypothesized that the energy metabolism of
126 RPE cells might be adapted to minimize consumption of glucose in order to
127 maximize the amount of glucose that can pass through the RPE to reach the
128 retina.

129 To examine glucose metabolism in RPE versus in retina, we compared two
130 preparations, mouse retina (mRetina) and cultured human fetal RPE cells
131 (hfRPE). The mouse retinas were freshly dissected from mouse eyes. The hfRPE
132 cells were grown 4-6 weeks in culture to form a monolayer with tight junctions
133 and a trans-epithelial resistance similar to native human RPE ($\geq 200 \Omega \cdot \text{cm}^2$). This
134 hfRPE preparation has been widely used to study RPE metabolism and to model
135 RPE-related diseases such as age-related macular degeneration due to its
136 similarity to native RPE cells (31-35). We added ^{13}C labeled glucose to both
137 preparations and then used mass spectrometry (7) to compare incorporation of
138 ^{13}C into glycolytic and TCA cycle intermediates. For these experiments we used
139 1,2 ^{13}C glucose because the pattern of ^{13}C labeling from this isotopomer can be
140 used to distinguish metabolites generated by glycolysis from metabolites
141 generated by the pentose phosphate pathway (36). Metabolites with one ^{13}C
142 ("m1") are generated from glucose that flows through the oxidative reactions of
143 the pentose phosphate pathway whereas metabolites with two ^{13}C ("m2") are
144 produced when glucose enters glycolysis directly. In a previous report we used
145 this labeling method to show that $< 2\%$ of the metabolic flux from glucose goes
146 through the pentose phosphate pathway in both mRetina and in hfRPE (9).

147 **Fig. 3A** shows the total pmoles per μg protein of several metabolites in mRetina
148 and in hfRPE. There are several striking differences. Lactate and succinate are

149 more abundant in mRetina than in hfRPE, whereas citrate and α -ketoglutarate
150 are more abundant in hfRPE than in mRetina. **Fig. 3B** shows the time course of
151 incorporation of ^{13}C into several key metabolites. The initial rate at which ^{13}C
152 from glucose incorporates into intracellular lactate in mRetina is at least 8 times
153 faster than in hfRPE. We also noted that the citrate and α -ketoglutarate pools are
154 larger and fill more gradually in hfRPE cells than in retina indicating a large
155 oxidative metabolic capacity of RPE mitochondria.

156 These findings support our hypothesis that a slow rate of conversion of glucose
157 to lactate in the RPE minimizes consumption of glucose so that more glucose
158 can reach the retina. In a previous study we showed that RPE cells further
159 minimize their use of glucose by using an alternative pathway known as
160 reductive carboxylation to make NADPH (9). We propose that limited production
161 of lactate and the use of reductive carboxylation to make NADPH are adaptations
162 of RPE cells that minimize their consumption of glucose so that more glucose
163 reaches the retina.

164 **RPE cells can use lactate as a fuel.** The retina converts most of the glucose it
165 consumes into lactate so we considered the possibility that RPE cells can use
166 retinal lactate as an alternative fuel source to compensate for their minimal
167 consumption of glucose, or even to further suppress glycolysis. We incubated
168 hfRPE cells either with U- ^{13}C glucose or with U- ^{13}C lactate for 5 or 10 minutes
169 and quantified incorporation of ^{13}C into glycolytic and TCA cycle metabolites. **Fig.**
170 **4A** shows that ^{13}C is incorporated rapidly into the pyruvate pool from both
171 glucose and lactate. However, in the citrate pools, ^{13}C from lactate accumulates
172 at least 20 times faster than ^{13}C from glucose. We also noted that substantial
173 amounts of m3 malate are formed. This shows that carboxylation of pyruvate is a
174 major metabolic pathway in hfRPE cells. **Fig. 4B** reports the time course of
175 incorporation of ^{13}C from lactate into TCA cycle intermediates in hfRPE cells.
176 Carboxylation of pyruvate occurs at about half the rate of decarboxylation of
177 pyruvate.

178 **Lactate can suppress consumption of glucose by RPE cells.** The results in
179 **Fig. 3** and **Fig. 4** show that glucose is consumed more slowly by RPE cells than
180 by retina. They also show that RPE cells efficiently use lactate for fuel as an
181 alternative to using glucose. Based on these findings we next asked whether
182 lactate can suppress consumption of glucose by RPE cells. We hypothesized
183 (**Fig. 5A**) that lactate dehydrogenase (LDH) in RPE cells depletes cytosolic NAD^+
184 when it oxidizes lactate to pyruvate. Since NAD^+ is required for glycolysis,
185 depletion of NAD^+ by lactate and LDH would suppress glycolysis so that RPE
186 cells consume less glucose.

187 We incubated hfRPE cell monolayers with 5 mM U- ^{13}C glucose either in the
188 absence or presence of 20 mM unlabeled lactate. We then harvested the cells
189 and used GC-MS to determine if lactate suppresses incorporation of ^{13}C from
190 glucose into glycolytic and TCA cycle intermediates.

191 The results of this experiment (**Fig. 5B**) show that unlabeled lactate substantially
192 increases the amounts of unlabeled pyruvate, citrate, isocitrate, fumarate and

193 malate (left panel of **Fig. 5B**). This is consistent with the results in **Fig. 4** showing
194 that carbons from lactate are incorporated rapidly into TCA cycle metabolites
195 through both carboxylation and decarboxylation of pyruvate.

196 Addition of lactate also causes accumulation of GAP, the triose phosphate
197 immediately upstream of the glyceraldehyde-3-phosphate dehydrogenase
198 (GAPDH) reaction, that requires NAD^+ . Consistent with this, added lactate
199 diminishes the amount of ^{13}C from glucose incorporated into intermediates
200 downstream of the GAPDH reaction (right side of **Fig. 5B**). Lactate does not
201 decrease incorporation of ^{13}C from glucose into m2 citrate and m2 isocitrate,
202 most likely because of anapleurotic supplementation of unlabeled TCA cycle
203 intermediates through pyruvate carboxylation enhanced TCA cycle activity (see
204 left side of **Fig. 5B**). Overall, lactate substantially inhibits glycolysis in hfrPE cells.

205 **Lactate can enhance transport of glucose across a monolayer of hfrPE**
206 **cells.** Next we asked whether lactate from photoreceptors can enhance the flow
207 of glucose across the RPE. We reasoned that suppression of glycolysis by
208 lactate minimizes consumption of glucose, so more glucose would cross from the
209 basolateral to the apical side of the RPE.

210 To test this idea, we measured the influence of lactate on transport of glucose
211 across a monolayer of hfrPE cells. We grew hfrPE cells on transwell filters to
212 confluence with a transepithelial resistance $\geq 200 \Omega \cdot \text{cm}^2$. We then added ^{13}C
213 glucose to the basolateral side, where the RPE normally would face the choroid
214 in an eye, and used mass spectrometry of the apical medium to quantify
215 transport of ^{13}C glucose to the apical side, where the RPE normally would face
216 the lactate-rich retina. We performed this experiment either with no added lactate
217 or with 1, 5, or 10 mM unlabeled lactate added to medium on the apical side (**Fig.**
218 **6A**). Consistent with our hypothesis, lactate added to the apical medium
219 substantially enhances transport of ^{13}C glucose from the basolateral to the apical
220 side of the hfrPE cells (**Fig. 6B**). Unlabeled lactate also suppresses the release
221 of ^{13}C lactate on the apical side (**Fig. 6C**).

222 **Long-term exposure to lactate enhances maturation of hfrPE cells.** Culture
223 conditions for hfrPE cells have been optimized for differentiation and for growth
224 (35). High concentrations of lactate generally are not included in culture media
225 for RPE cells. However, in their native environment within a living eye, RPE cells
226 normally would be exposed to constantly high concentrations of lactate released
227 from the retina.

228 Since lactate is metabolized efficiently by hfrPE cells we hypothesized that the
229 presence of lactate in the culture medium might influence their differentiation
230 state. To test this we incubated hfrPE cells in standard medium containing
231 glucose until they were confluent and had achieved a trans-epithelial resistance
232 $\geq 200 \Omega \cdot \text{cm}^2$. We then lowered the concentration of glucose to 0.5 mM and
233 added 10 mM lactate. Remarkably, cell survival was excellent. After 21 days
234 pigmentation of the lactate supplemented hfrPE cells increased substantially
235 compared to control hfrPE cells provided with standard 5 mM glucose sans
236 lactate. (**Fig 7A**). **Fig. 7B** shows that the levels of several key metabolic enzymes

237 decreased, whereas the ratio of IDH3 to other IDH isoforms increased. Exposure
238 to lactate also alters metabolic flux through decarboxylation and carboxylation of
239 pyruvate (**Fig. 7C**) and reductive carboxylation (**Fig. 7D**). A more complete
240 analysis of the effects of lactate on RPE cell differentiation is needed, but our
241 initial findings, shown here, demonstrate that lactate not only supports RPE
242 metabolism, but it also influences the differentiation state of RPE cells.

243 **Metabolic specializations of the retina and RPE decline with age.** The
244 analyses of RPE metabolism in this study focused on the cultured hRPE, which
245 is a well characterized model that has been used to evaluate RPE metabolism
246 (32). hRPE cells have been used as a cell culture model for studying various
247 diseases, including age-related macular degeneration (34). The RPE cultures
248 used in the experiments reported here are of a similar age in culture as the ones
249 used in other published studies, including those modeling AMD.

250 However, to confirm that the metabolic differences between retina and hRPE are
251 similar to the differences between retina and RPE in an eye, we used a mouse
252 eyecup preparation with retinas removed to confirm the basic metabolic features
253 that we identified in this study. We incubated freshly separated retinas and
254 eyecups in medium containing glucose and glutamine and then analyzed
255 metabolites by GC-MS. **Fig. 7E** compares the ratio of total lactate to total citrate
256 in the retina vs. in the eyecup. Similar to the ratio we found for mouse retina and
257 hRPE, the lactate/citrate ratio is ~30 times higher in retina than in the eyecup.

258 Based on our findings we speculated that degeneration of photoreceptors in
259 response to mutations or to aging could be influenced by the metabolic
260 relationship between the retina and RPE. The eyecup preparation allowed us to
261 examine the effect of aging on the lactate/citrate ratio in retina and RPE. **Figs.**
262 **7E and 7F** show that lactate/citrate in the retina *decreases* substantially as mice
263 age from 6 months to 32 months. In contrast, lactate/citrate *increases* with age in
264 the eyecup. In other words the retina becomes less glycolytic with aging while the
265 eyecup, containing the RPE layer, becomes more glycolytic. These results
266 suggest that the specialized metabolic features, that are fundamental to the
267 retina-RPE ecosystem, decline with age both in the retina and in the RPE and
268 that this decline could contribute to age-related vision loss (37, 38).

269

270

271 **DISCUSSION**

272 **Model for a network of metabolic interdependence between the retina and**
273 **RPE. Fig. 8** summarizes our model for the retina-RPE metabolic ecosystem.
274 Lactate from photoreceptors suppresses glycolysis in the RPE so more glucose
275 can reach the retina.

276 **Previous evidence that cells in the retina have specific metabolic roles.** The
277 distributions of metabolic enzymes in mouse retina indicate that photoreceptors
278 have the enzymes and transporters they need for glycolysis, but MGCs do not.
279 Glycolysis requires pyruvate kinase (PK). The M2 isoform of PK (PKM2) is highly
280 enriched in photoreceptors (10, 18-20, 39), but MGCs do not express substantial
281 amounts of any PK isoform (10). MGCs also do not express hexokinase (20).
282 Furthermore, lactate, rather than glucose, is the most effective source (10) of
283 carbon for glutamine synthesis by MGCs (40) in mouse retinas. Based on these
284 observations, we proposed that MGCs in a retina primarily use lactate produced
285 by photoreceptors (41). Together with the results described in this report it
286 appears that the central role of photoreceptors in retinal energy metabolism is to
287 convert glucose to lactate, which then is used as fuel by both RPE and Müller
288 cells.

289 **Significance of aerobic glycolysis in the retina.** Enhanced capacity for
290 anabolic metabolism has been proposed as the purpose of aerobic glycolysis in
291 photoreceptors (10, 18, 19), but our model suggests an additional purpose. We
292 propose that the laminated structure of the eye, in which the RPE separates the
293 retina from its source of nutrients, requires photoreceptors to produce and
294 release lactate to suppress glycolysis so that sufficient glucose can flow through
295 the RPE.

296 **The “retinal ecosystem” model helps to explain recent findings from**
297 **genetic manipulations of photoreceptors and RPE.** Engineering
298 photoreceptors to be more glycolytic makes them more robust, whereas
299 engineering RPE cells to be more glycolytic causes photoreceptors to
300 degenerate (3, 21-23). The model shown in **Fig. 8** provides an explanation for
301 those seemingly opposing findings. When photoreceptors are engineered to be
302 more glycolytic they produce more lactate that can more substantially suppress
303 glycolysis in the RPE. In this way more glucose reaches the retina, thereby
304 enhancing photoreceptor survival. When the RPE is more glycolytic it consumes
305 more glucose, leaving less glucose available for the retina so photoreceptors
306 starve and become stressed.

307 **The concept of a metabolic ecosystem and its relationship to retinal**
308 **disease.** The “retina ecosystem” model in **Fig. 8** suggests an explanation for the
309 linkage between Age-Related Macular Degeneration and accumulation of
310 mitochondrial DNA damage in RPE cells (42). Photoreceptors may starve when
311 RPE mitochondria fail because the RPE becomes more dependent on glycolysis,
312 which prevents glucose from reaching the retina.

313 The concept of a metabolic ecosystem also has implications for other types of
314 retinal disease. Mutations that affect genes expressed only in rods can cause

315 rods to degenerate. However, cones subsequently degenerate as a
316 consequence of the loss of rods, even though the cones are not affected directly
317 by the mutant gene (43). One reason for this is that loss of a cone viability factor
318 that normally is produced by rods may contribute to cone degeneration in this
319 type of disease state (44). The model in **Fig. 8** suggests another factor that also
320 can contribute to the secondary loss of cones when rods degenerate. A retina
321 without rods makes less lactate (8). We have shown in this report that, without
322 lactate to suppress glycolysis, RPE cells oxidize more glucose and transport less.
323 In a rod-less retina the loss of lactate production would limit the rate at which
324 glucose can be supplied to cones. This can explain why cones starve (2) and
325 why 2-NBDG accumulates in RPE cells (45) when rods degenerate. Consistent
326 with this explanation, cones in these retinas can be rescued from degeneration
327 by supplementation with an alternative supply of glucose (45).

328 **Other fuels also may contribute in the metabolic ecosystem.** This study
329 highlights one way that RPE, photoreceptors and MGCs can work together as an
330 ecosystem of metabolically specialized interdependent cells. Our investigation
331 focused on glucose and lactate, but it is very likely that fatty acids, ketone bodies,
332 (46-48) and metabolites from other metabolic pathways (20) also contribute
333 significantly to this metabolic ecosystem. For example, oxidation of fatty acids by
334 the RPE can supply the retina with ketone bodies (46). Furthermore, a recent
335 study showed that RPE oxidizes fatty acids from photoreceptor phagocytosis,
336 (48) which also can suppress the need for RPE cells to consume glucose.
337 Together these studies suggest that energy homeostasis in retina and RPE relies
338 on a specialized metabolic interplay that could form the basis of future therapies
339 for a range of retinal degenerative diseases.

340

341 **MATERIAL AND METHODS**

342 **Animals.** All research was authorized by the University of Washington
343 Institutional Animal Care and Use Committee. Mice in the C57BL6 background
344 were maintained in the University of Washington South Lake Union vivarium at
345 27.5 °C on a 14h/10h light-dark cycle. Transgenic mice expressing eGFP under
346 the Nrl promoter (49) (RRID:IMSR_JAX:021232), or tdTomato under the Rlbp-
347 CRE promoter (28) were described previously. Aged mice (6 month and 32
348 month) were C57BL/6J. This strain does not carry the rd8 mutation in the Crb1
349 gene (50).

350 Transgenic heterozygote zebrafish in the AB background were maintained in the
351 University of Washington South Lake Union aquatics facility at 27.5 °C on a
352 14h/10h light-dark cycle. Fish used for experiments were male and female
353 siblings between 12-24 months old. A transgenic line stably expressing tdTomato
354 in Müller cells (GFAP:tdTomato; RRID:ZDB-FISH-150901-17843) was described
355 previously (30). Prior to gavage experiments, fish were fasted >18 h and dark-
356 adapted >12 h.

357 **Antibodies.**

358 Arrestin1, D9F2 (from Larry Donoso and Cheryl Craft)
359 IHC: 1:200

360 GLUT1, (AbCam, ab115730; RRID:AB_10903230)
361 IB: 1:200,000, 0.86 ng/ml;
362 IHC 1:1000, 0.17 mg/ml
363 GLUT3, (AbCam, ab41525; RRID:AB_732609)
364 IB: 1:5000, 0.136 ug/ml
365 GLUT4, (AbCam, ab654; RRID:AB_305554)
366 IB: 1:5000
367 Glutamine synthetase, (Millipore, MAB302; RRID:AB_2110656)
368 IHC: 1:1000
369 MTCO1 (Abcam, ab14705; RRID:AB_2084810)

370 **Tissue preparations for immunoblotting.** Frozen tissue samples were
371 homogenized in RIPA buffer (150 mM NaCl, 1% Triton X-100, 0.05% sodium
372 deoxycholate, 0.1% SDS, 50 mM Tris, pH 8.0 with a mixed
373 phosphatase/protease inhibitor cocktail (ThermoFisher 88668), briefly sonicated,
374 then rocked at 4°C for 30min. Samples were then spun at 13,300 RPM at 4°C for
375 15 min, and the supernatant was normalized for loading by BCA assay to 20
376 mg/tissue. RPE protein lysate was prepared according to a described protocol
377 (51).

378 To prepare membrane fractions, frozen tissue samples were homogenized in
379 PBS (0.14 M, pH 7.4) with a mixed phosphatase/protease inhibitor cocktail, then
380 rocked at 4°C for 30 min. Samples were then spun at 45,000 rpm at 4°C, the
381 supernatant (cytosolic fraction) drawn off and saved, and the pellet (membrane
382 fraction) was resuspended in an equal volume of PBS. After mixing with 5X
383 Laemmli loading buffer, 1 ml benzonase (Millipore 70746) was added. Each
384 tissue was then loaded with equal volumes of cytosolic and membrane fraction.

385 **Immunoblotting.** Samples were run on 12%, self-cast acrylamide gels and
386 transferred onto PVDF membranes (Millipore IPFL00010). Following protein
387 transfer, membranes were blocked with LI-COR Odyssey Blocking Buffer (LI-
388 COR, 927-40000) for 1 h at room temperature. Primary antibodies were diluted in
389 blocking buffer and incubated overnight at 4°C. Membranes were washed,
390 incubated with secondary antibody (LI-COR IRDye 800CW, 926-32210,
391 (RRID:AB_621842), and 926-32211, (RRID:AB_621843), 1:5000 1h at room
392 temperature, and washed again. Imaging was performed using the LI-COR
393 Odyssey CLx Imaging System (RRID:SCR_014579).

394 **Immunohistochemistry:** Retinal eyecups were micro-dissected from C57BL6J
395 mice and were fixed in 4% paraformaldehyde in PBS, rinsed with PBS, incubated
396 in a sucrose gradient (5%, 10%, and 20%), embedded into OCT and
397 cryosectioned at 20µm. Mouse sections were washed in PBS, then blocked in
398 IHC buffer (5% normal donkey serum diluted in PBS with 2 mg/mL BSA and
399 0.3% Triton X-100) for 1 h. Primary antibodies were diluted in IHC blocking buffer
400 as specified, and applied to blocked cryosections overnight at 4°C. Secondary
401 antibodies were diluted at 1:3000 in IHC blocking buffer, and applied to mouse
402 retina sections for 1 h in darkness. Sections were washed in PBS three times,
403 and mounted with SouthernBiotech Fluoromount-G (Fisher Scientific) under
404 glass coverslips and visualized using a Leica SP8 confocal microscope with a

405 63X oil objective. Images were acquired at a 4096x4096 pixel resolution with a
406 12-bit depth using Leica LAS-X software (RRID:SCR 013673).

407 **RPE cell culture.** Human fetal eyes with a gestational age of 16-20 weeks
408 were harvested and shipped overnight on ice in RPMI media containing
409 antibiotics from Advanced Bioscience Resources Inc. (Alameda, CA).
410 Dissections of fetal tissue were performed within 24 hours of procurement and
411 followed a modified version of the dissection protocol in order to isolate the
412 retinal pigment epithelium (RPE) (35). The fetal RPE sheets were incubated at
413 37°C with 5% CO₂ and cultured in RPE media. The RPE media consisted of
414 Minimum Essential Medium alpha (Life Technologies) supplemented with 5%
415 (vol/vol) fetal bovine serum (Atlanta Biologicals), N1-Supplement (Sigma-Aldrich),
416 Nonessential Amino Acids (Gibco), and a Penicillin-Streptomycin solution (Gibco).
417 Isolated fetal RPE reached confluency about 3-4 weeks after dissection and was
418 then passaged using a 0.25% Trypsin-EDTA solution (Gibco) and passed
419 through a 40 mm nylon cell strainer (BD Falcon) in order to collect a suspension
420 of single cells. After counting, the RPE cells were plated onto 0.3 cm² cell culture
421 inserts (Falcon) coated with Matrigel (Corning) at a seeding density of 100,000
422 cells per insert. Cells grown on these inserts were cultured in RPE media
423 containing 1% (vol/vol) FBS. Transepithelial resistance was measured weekly
424 after 2 weeks in culture using a Millicell ERS-2 Epithelial Volt-Ohm Meter
425 (Millipore).

426 **Oral Gavage.** Mice were fasted overnight in the dark, and gavaged the next
427 morning in ambient light. A micro-syringe fitted with a 22 gauge 1.5" straight 1.25
428 mm ball-tip needle was used to orally administer 100 µl of 50 mM 2-NBDG
429 (Invitrogen) dissolved in water. Successfully gavaged mice were returned to
430 darkness during the 2-NBDG incubation period.

431 Zebrafish were gavaged using methods described previously(52) under red light.
432 Briefly, overnight fasted adult zebrafish were anaesthetized > 1 min with 150
433 mg/mL MS-222 in fish water. Fish were placed in a slit cut in a cellulose sponge
434 soaked with MS-222 solution, and the sponge was rotated to orient the fish
435 mouth up. A micro-syringe fitted with thin, flexible 1 mm OD plastic tubing was
436 used to orally administer 5 µL of either fish water or 30 mM 2-NBDG (Invitrogen).
437 Gavaged fish were immediately placed into a recovery tank of fresh fish water
438 and monitored briefly using a UV flashlight for regurgitation of 2-NBDG.
439 Successfully gavaged fish were returned to darkness during the 2-NBDG
440 incubation period.

441 **Tissue slicing and imaging.** Gavaged mice were euthanized by asphyxiation
442 with CO₂. Zebrafish were euthanized in an ice bath followed by cervical
443 dislocation. Euthanized animals were enucleated, and the retinas dissected away
444 under red light into cold Ringer's solution (133 mM NaCl, 2.5 mM KCl, 1.5 mM
445 NaH₂PO₄, 2 mM CaCl₂, 1.5 mM MgCl₂, 10 mM HEPES, 10 mM D-glucose, 1 mM
446 sodium lactate, 0.5 mM L-glutamine, 0.5 mM reduced glutathione, 0.5 mM
447 sodium pyruvate, 0.3 mM sodium ascorbate, pH 7.4). Isolated retinas were
448 mounted on filter paper (0.45 µm pore, mixed cellulose, Millipore) and flattened
449 with gentle suction. After peeling away remaining RPE, flat-mounted retinas were

450 sliced into 300-400 μm slices using a tissue slicer (Stoelting). Slices were rotated
451 90° and the filter paper edges buried in strips of wax on a coverslip for imaging at
452 room temperature. Fresh retinal slices were imaged at room temperature using a
453 Leica SP8 confocal microscope with a 40X water objective; excitation/emission
454 wavelengths were 488/525-575 nm for 2-NBDG, and 559/580-630 nm for
455 tdTomato. Leica LAS-X (RRID:SCR_013673) software was used to acquire
456 images at 2048 x 2048 pixel resolution with 12 bit depth, and Z-stacks imaged
457 every 0.5 μm over a tissue depth of 10-30 μm .

458 **Image analysis.** ImageJ software (RRID:SCR_002285) was used for
459 quantification of 2-NBDG fluorescence in fresh retinal slices. 10 slices of each Z-
460 stack were maximum intensity projected, and retinal layers were identified by
461 morphology and expression of transgenic markers. For every slice, 3 small
462 uniformly sized rectangular regions of interest (ROIs) were placed randomly in
463 each retinal layer, and mean fluorescence intensity of each ROI was measured.
464 Average 2-NBDG fluorescence in each layer was divided by the
465 autofluorescence of corresponding retinal layers from animals gavaged with
466 saline or water.

467 **Metabolic flux analysis:** Isolated mouse retina or confluent human fetal RPE
468 cells were changed into pre-warmed Krebs-Ringer Bicarbonate Buffer containing,
469 depending on the experiment, [1,2] ^{13}C glucose, U- ^{13}C glucose, U- ^{13}C lactate or
470 U- ^{13}C glutamine (Sigma) as described elsewhere (5, 7, 9). Both retinas and RPE
471 cells were incubated for 5 min, 30 min, 60 min and 120 min. Metabolites from
472 each time point were extracted and analyzed by gas chromatography mass
473 spectrometry (GC-MS, Agilent 7890/5975C) as described in detail (5, 6).

474 **Measurement of U- ^{13}C glucose transport across hRPE cells on transwell**
475 **filters.** After maturation for 4-6 weeks in culture, hRPE cells grown on transwell
476 filters were changed into 500 ml of DMEM containing 1% FBS on each side. 5.5
477 mM U- ^{13}C glucose (Cambridge Isotope Laboratories) was included in the
478 medium in the basolateral side while various concentrations of sodium lactate
479 was added to the apical side, while maintaining a constant pH. Apical side
480 medium was collected at 8 and 24 h to analyze the transported U- ^{13}C glucose by
481 liquid chromatography coupled with triple quadrupole mass spectrometry (Waters
482 Xevo TQ Tandem mass spectrometer with a Waters ACQUITY system with
483 UPLC) as reported in detail (7).

484 **Serial Block Face Scanning SEM**

485 Mouse eyes were enucleated, the anterior half was dissected away, and the
486 eyecup was cut in half. Tissue was fixed in 4% glutaraldehyde in 0.1 M sodium
487 cacodylate buffer, pH 7.2, at room temperature (RT), then stored overnight at
488 4°C . Samples were washed 4 times in sodium cacodylate buffer, postfixed in
489 osmium ferrocyanide (2% osmium tetroxide/3% potassium ferrocyanide in buffer)
490 for 1 h on ice, washed, incubated in 1% thiocarbohydrazide for 20 min, and
491 washed again. After incubation in 2% osmium tetroxide for 30 min at RT,
492 samples were washed and en bloc stained with 1% aqueous uranyl acetate
493 overnight at 4°C . Samples were finally washed and en bloc stained with Walton's
494 lead aspartate for 30 min at 60°C , dehydrated in a graded eth- anol series, and

495 embedded in Durcupan resin. Serial sections were cut at 60 nm thickness and
496 imaged with 6 nm pixel size using a Zeiss Sigma VP scanning electron
497 microscope fitted with a Gatan 3View2XP ultramicrotome apparatus. Imaged
498 stacks were concatenated and aligned using TrakEM2 (RRID:SCR_008954).
499 Unless stated otherwise, five washes with water were used for all wash steps.

500 **Statistical analyses.**

501 R (RRID:SCR_001905) with R Commander was used to perform one-way
502 ANOVA for NBDG gavage experiments.

503 **Reproducibility.** All data shown here have been reproduced at least three times
504 by the authors.

505 **Data availability.** All data supporting the findings of this study are available
506 within the paper.

507

508

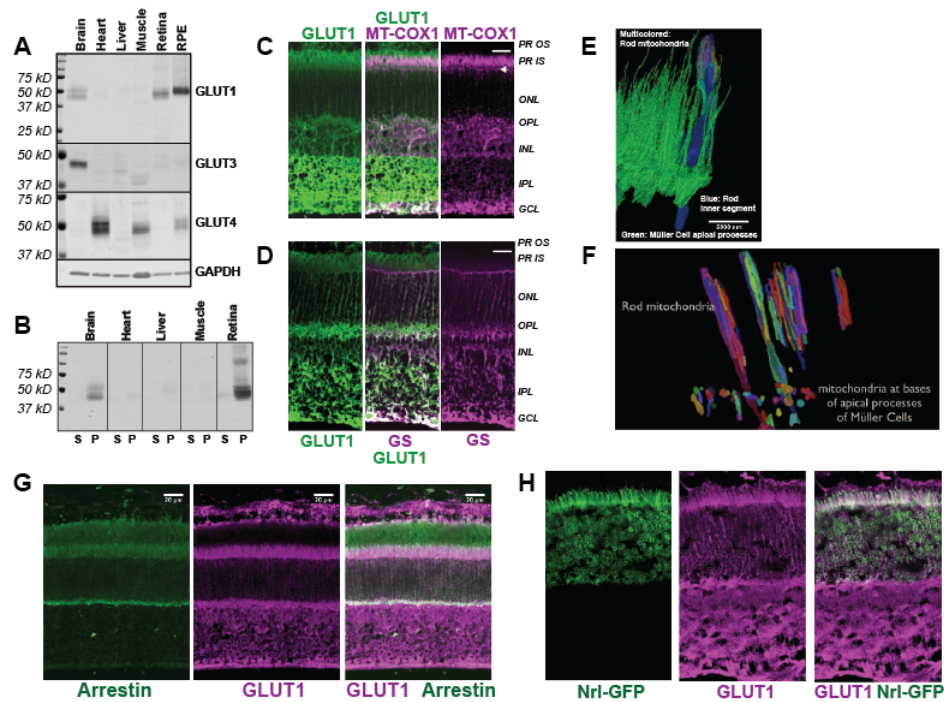
509

510

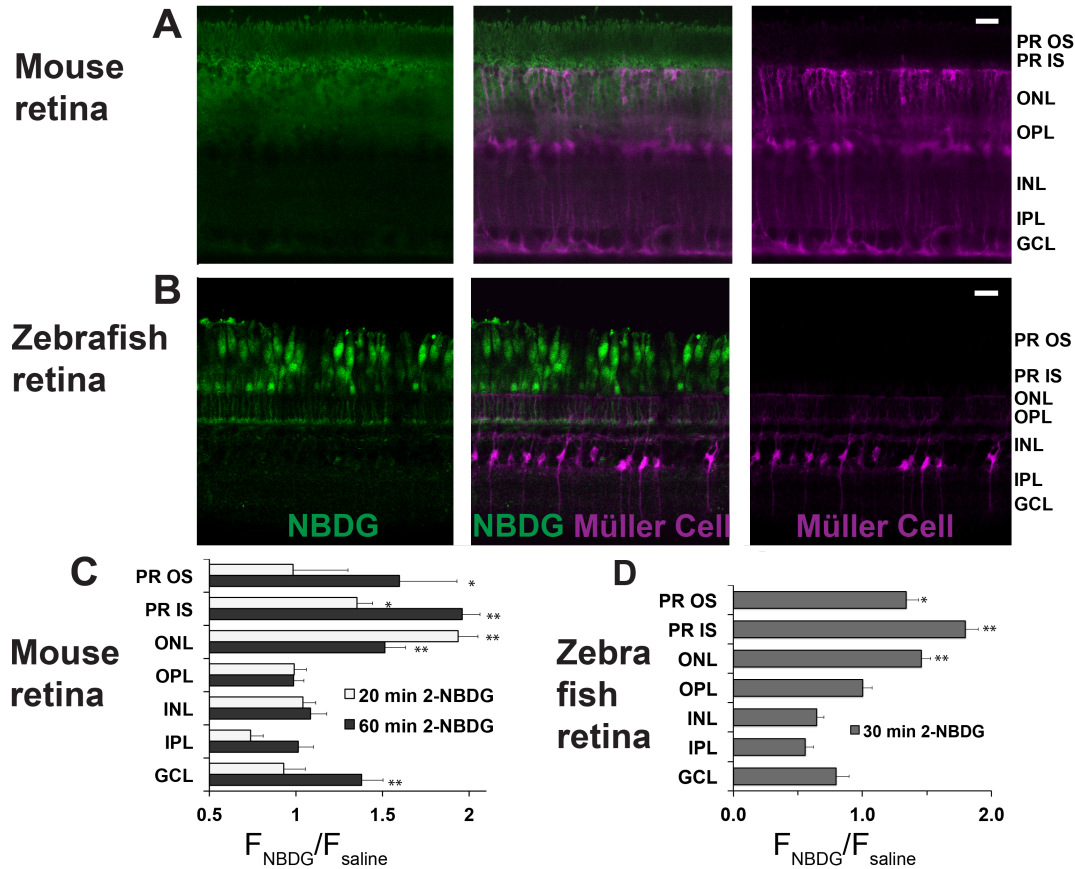
511

512 **Acknowledgements.** This study was supported by funding from NIH EY06641
513 and NIH EY017863 to JBH, NIH EY026020 to SEB and from NEI core grant
514 EY001730.

515



516
 517 **Fig. 1. Distribution of GLUT1 in retina.** **A.** Immunoblot analysis of mouse tissue
 518 homogenates confirms that GLUT-1 is the primary glucose transporter in mouse
 519 retina and RPE. 1 μ g total homogenate protein was loaded in each lane. No
 520 antibodies that we could validate were available for GLUT2. However, the
 521 Human Protein Atlas reports no expression of GLUT2 in retina (53). **B.** Evidence
 522 that the protein immunoreactive with the GLUT-1 antibody is membrane
 523 associated. Homogenates were centrifuged and equivalent percentages of total
 524 supernatant (S) and total pellet (P) were probed with the GLUT-1 antibody. **C.**
 525 GLUT1 in mouse retina. Rods inner segments are identified by the unique
 526 morphology of their mitochondria labeled with mitochondrial cytochrome oxidase
 527 1 antibody (MT-COX1). White arrowhead indicates the layer of Müller cell
 528 mitochondria. **D.** Müller cells are identified by glutamine synthetase (GS)
 529 immunoreactivity. Scale bars represent 20 μ m. **E.** Serial Block Face Scanning
 530 Electron Microscopy. The inner segment of one rod cell is shown in blue with its
 531 mitochondria shown as multi-colored. The green structures are apical processes
 532 of MGCs. **F.** Differences in location and morphology between rod mitochondria
 533 and MGC mitochondria in mouse retina. For clarity not all of the mitochondria are
 534 shown. MGC mitochondria are located just below the outer limiting membrane. **G.**
 535 The left panel shows labeling of rods in a partially light-adapted mouse retina
 536 with a rod arrestin antibody. The middle panel shows labeling with a GLUT1
 537 antibody and the right panel shows the merge. **H.** The left panel shows
 538 expression of GFP from the rod-specific Nrl promoter. The middle panel shows
 539 labeling with a GLUT1 antibody and the right side shows the merge. PR OS,
 540 photoreceptor outer segment; PR IS photoreceptor inner segment; ONL, outer
 541 nuclear layer; OPL, outer plexiform layer; INL inner nuclear layer; IPL inner
 542 plexiform layer; GCL, ganglion cell layer.



543

544

545

546 **Fig. 2. Fluorescent glucose (2-NBDG) accumulates in photoreceptors after**

547 **oral gavage. A.** 2-NBDG (green) accumulation in a mouse retina 20 min. after

548 oral gavage. MGCs are identified by tdTomato in cells in which the Rlbp1

549 promoter is active. **B.** 2-NBDG accumulation in a zebrafish retina 30 min after

550 oral gavage. MGCs are identified by tdTomato expressed from the GFAP

551 promoter. Labels on the right of panels A and B represent approximate positions

552 of the retinal layers, **C.** Quantification of 2-NBDG fluorescence from mouse

553 retinas (n = 5 animals, 17 slices for 20 min 2-NBDG; 3 animals, 8 slices for 1 h 2-

554 NBDG; 3 animals, 8 slices for saline). $F_{\text{NBDG}}/F_{\text{saline}}$ compares fluorescence from

555 retinas of mice gavaged with 2-NBDG vs. with saline. Error bars report SEM. **D.**

556 Quantification of 2-NBDG fluorescence from zebrafish retinas (3 animals, 8 slices

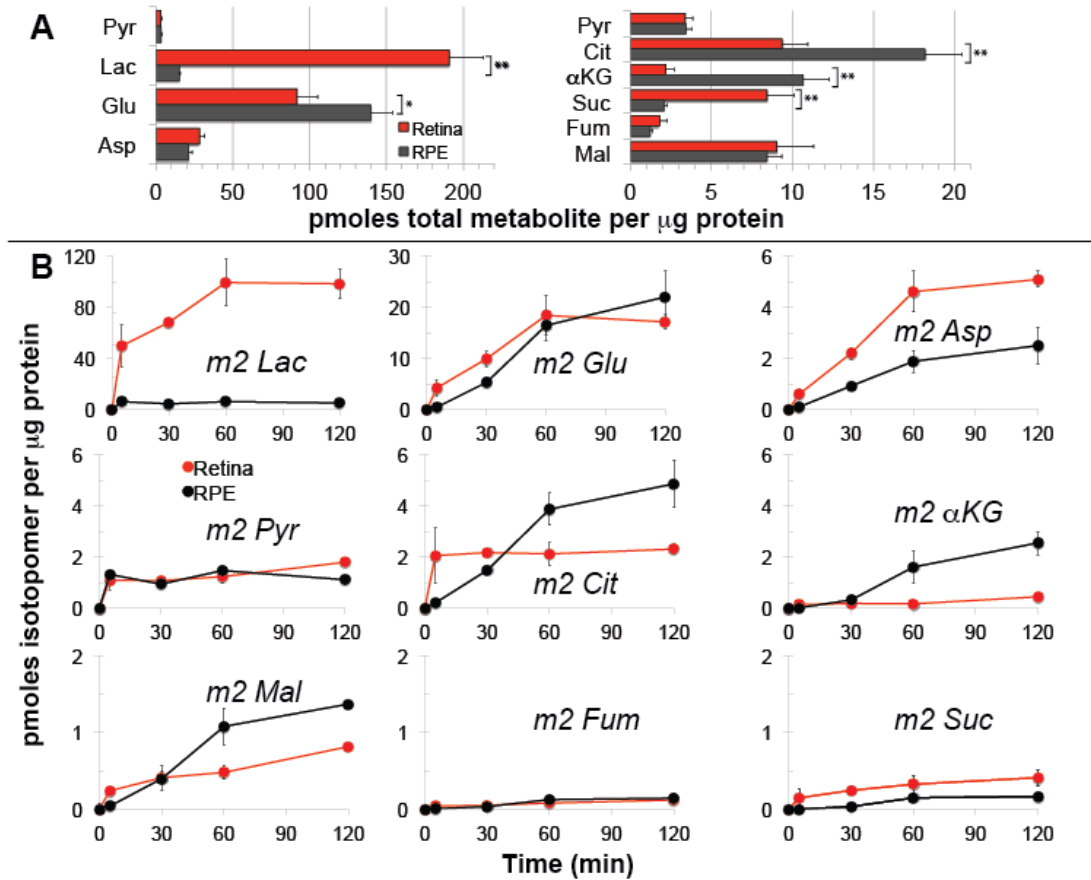
557 for 30 min 2-NBDG; 2 animals, 3 slices for saline). PR OS, photoreceptor outer

558 segments; PR IS, photoreceptor inner segments; ONL, outer nuclear layer; OPL,

559 outer plexiform layer; INL, inner nuclear layer; IPL, inner plexiform layer; GCL,

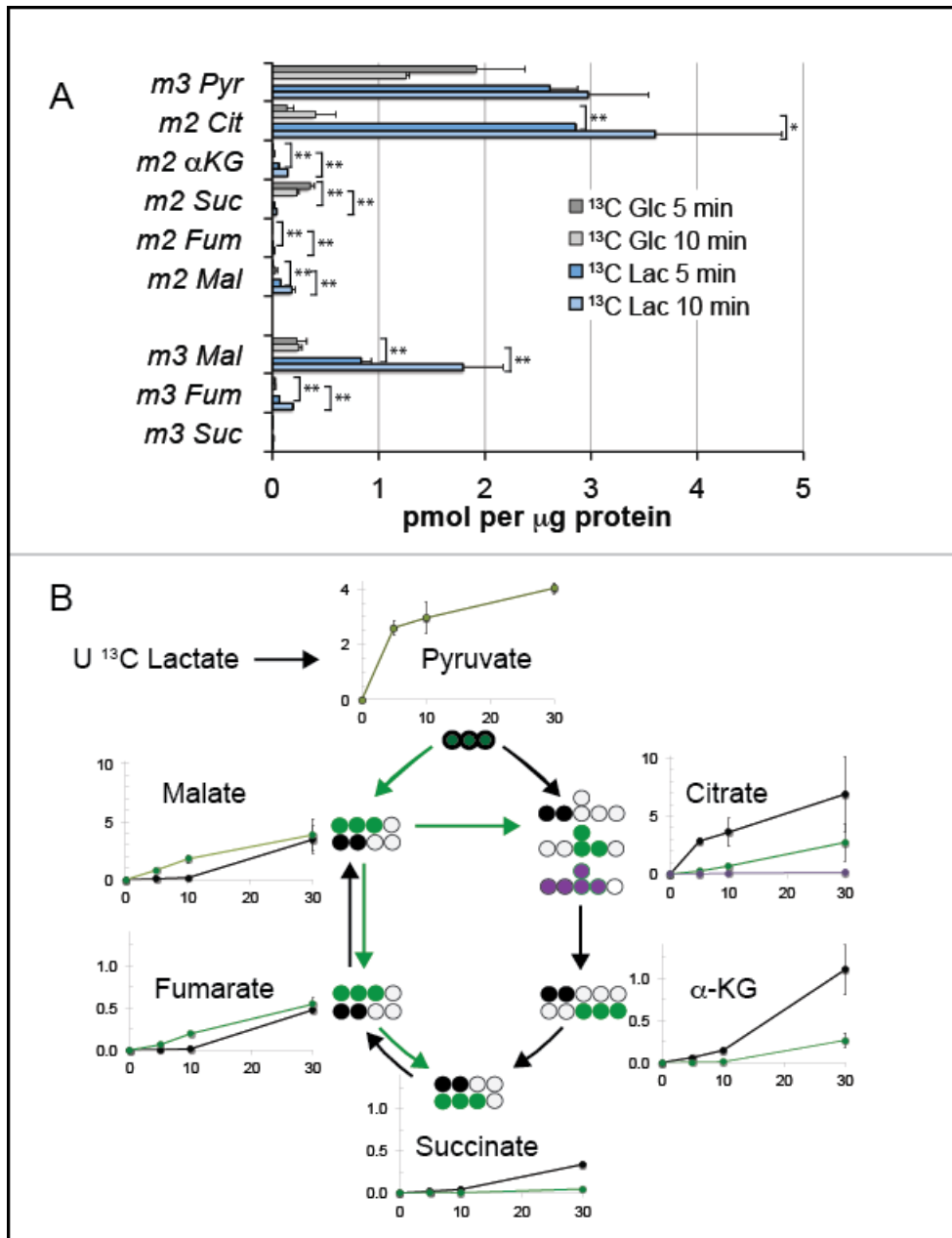
560 ganglion cell layer. Scale bars represent 20 μm . * indicates $p < 0.05$ and **

561 indicates $p < 0.01$ for the comparison of F_{NBDG} to F_{saline} .



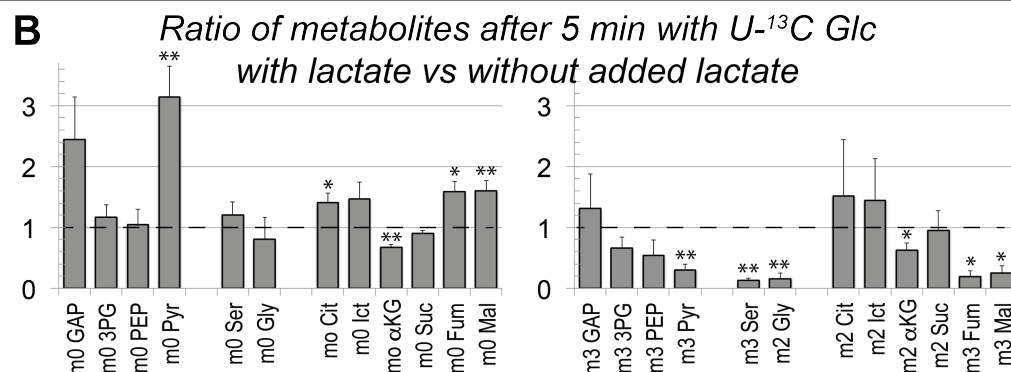
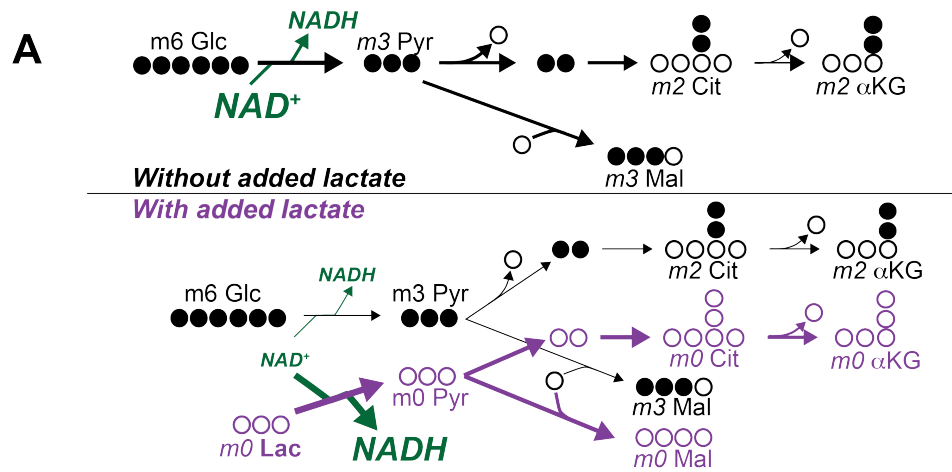
562
563
564
565
566
567
568
569
570

Fig. 3. Differences in metabolic flux in retina and RPE. A. Total metabolite levels (pmoles per µg protein) in mRetina (red) and hfRPE (black). (n = 11) Note the different scales for the left and right panels. **B.** Incorporation of ¹³C from [1,2]¹³C glucose into metabolites in mRetina and hfRPE cells (pmoles per µg protein). Each of the isotopomers shown is derived from glucose metabolized by glycolysis. Note the different scales for the top, middle and bottom panels. (n = 3 for each time point; error bars represent standard deviation).

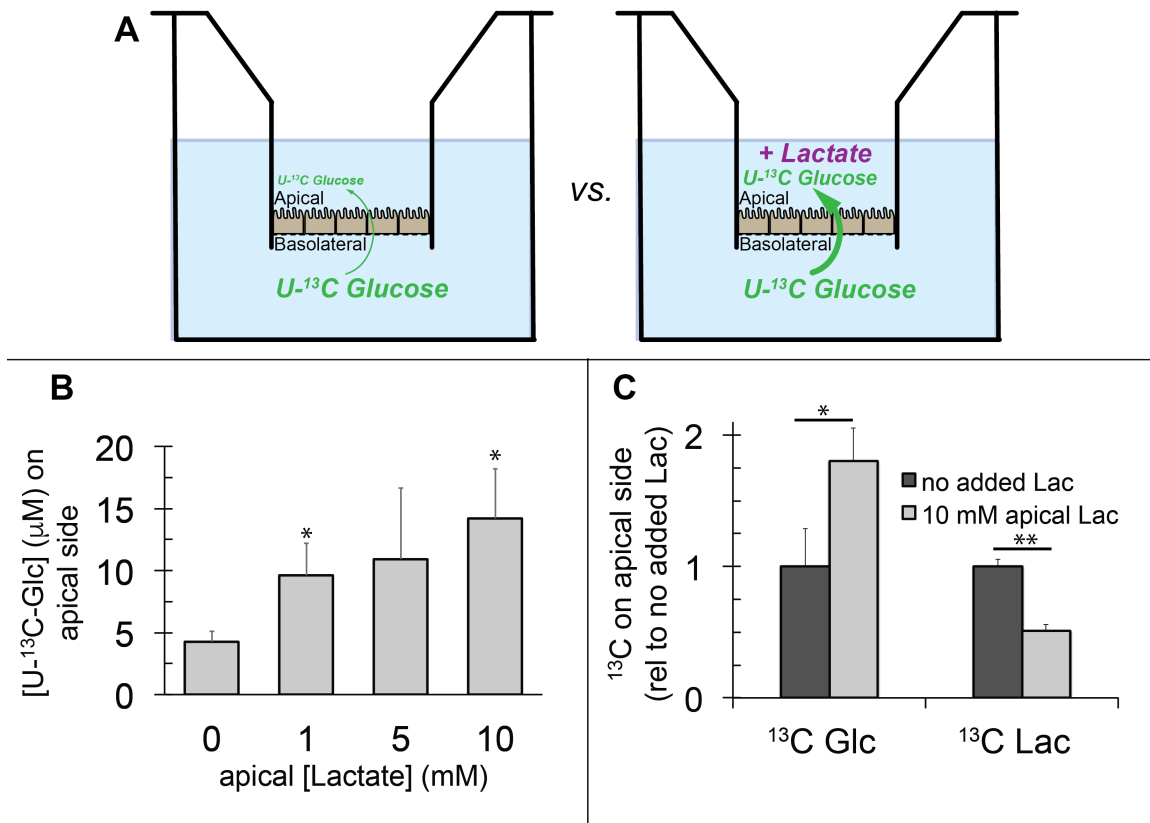


571
572
573
574
575
576
577
578
579

Fig. 4. Incorporation of ^{13}C from lactate into metabolic intermediates in hRPE cells. **A.** Comparison of initial rates of labeling (at 5 and 10 minutes after introduction of labeled fuel) from U- ^{13}C glucose vs. from U- ^{13}C lactate. Citrate and malate take up label faster from lactate than from glucose. **B.** Time courses of incorporation of ^{13}C from U- ^{13}C lactate into hRPE metabolites accompanied by schematic illustrations of the labeled species in the context of the TCA cycle. (n = 2-3 for each time point; error bars represent range or standard deviation).

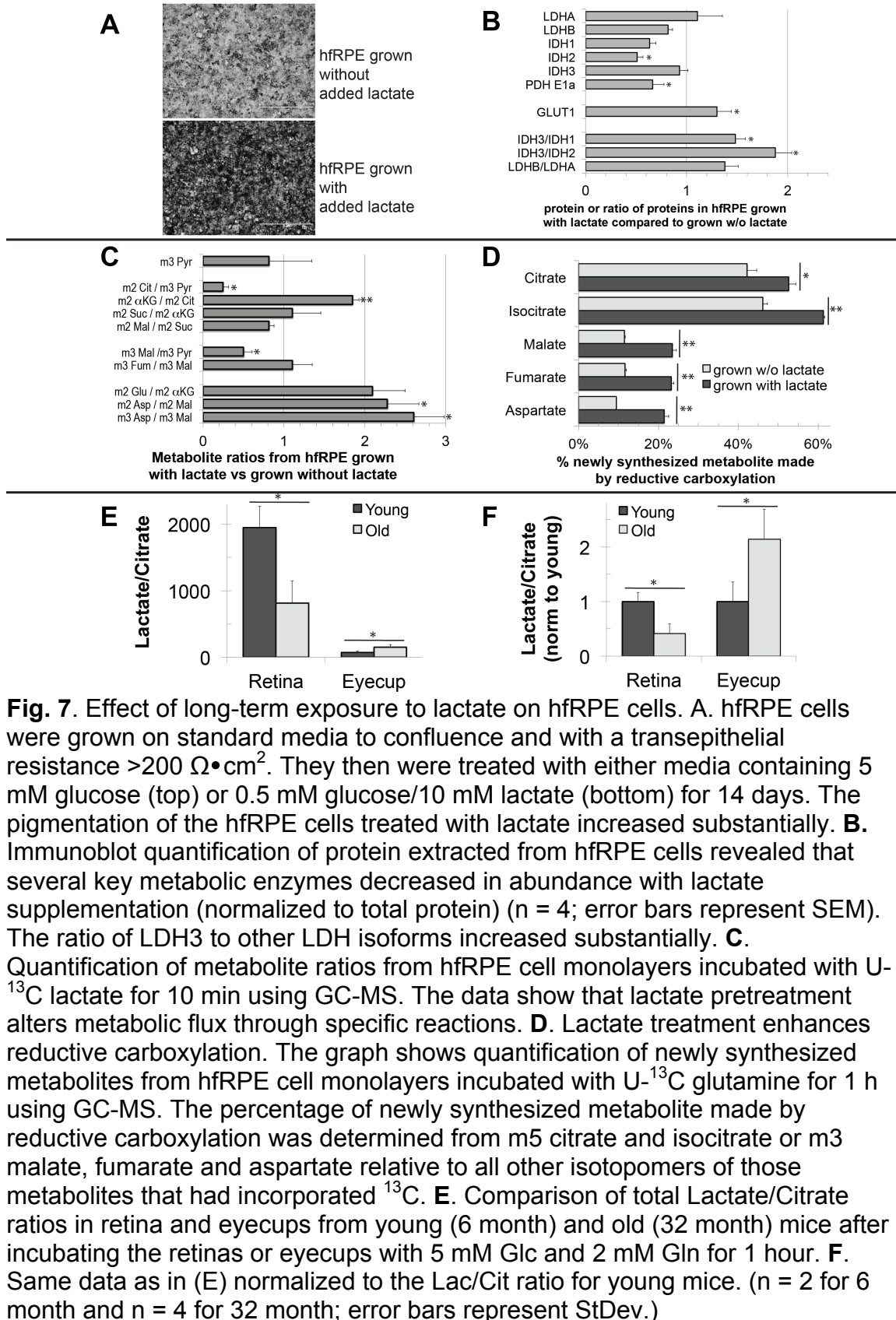


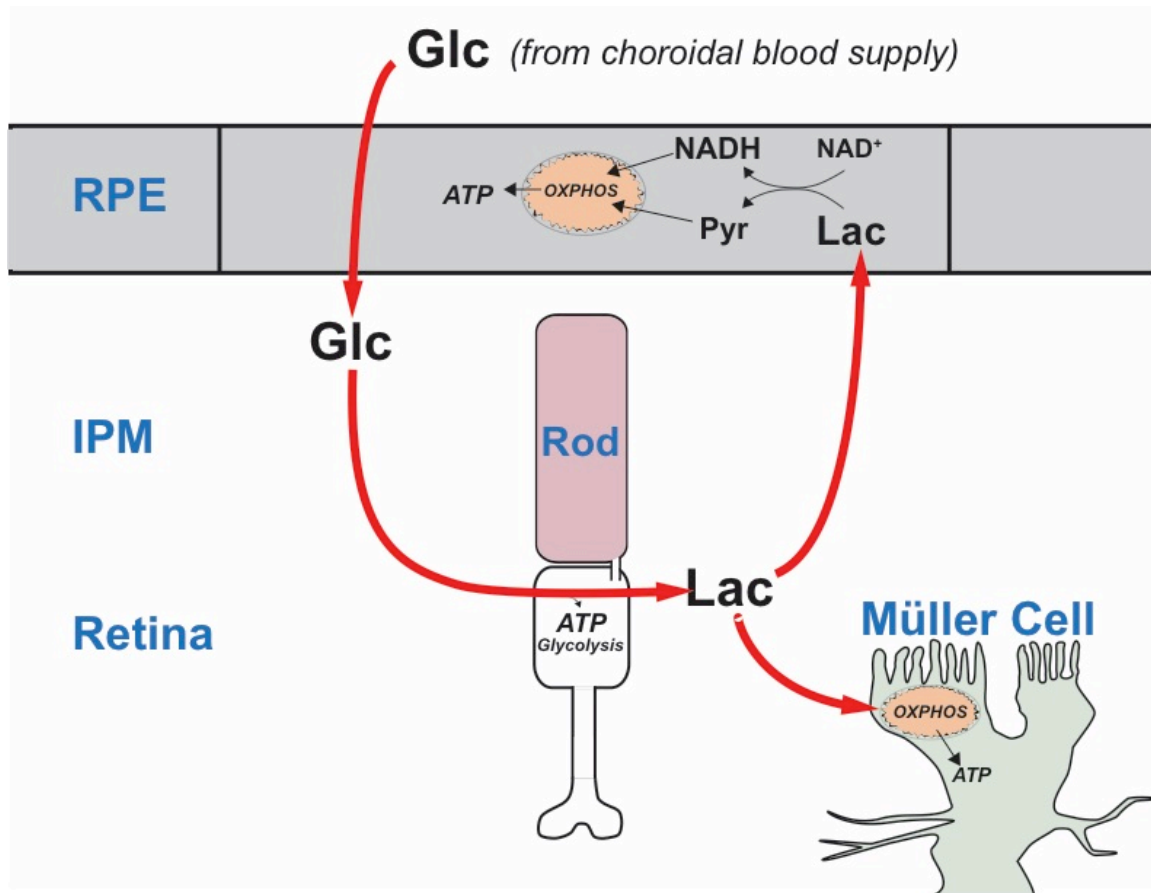
580
 581 **Fig. 5. Lactate suppresses oxidation of glucose by hRPE cells. A.**
 582 Schematic prediction of how U-¹³C Glc (“m6 Glc”) would be metabolized without
 583 lactate (top) vs. with lactate (bottom). We hypothesized that lactate would
 584 suppress glycolysis of m6 Glc by depleting NAD⁺. The model also predicts that
 585 unlabeled (m0) pyruvate and TCA cycle intermediates become more abundant. **B.**
 586 Experimental results showing that lactate substantially increases the total
 587 amounts of unlabeled (m0) GAP, pyruvate, citrate, isocitrate, fumarate and
 588 malate (left panel) in hRPE cells. The right panel shows that 20 mM lactate
 589 suppresses the incorporation of ¹³C from 5 mM ¹³C Glc into glycolytic and TCA
 590 intermediate. (n = 3; error bars represent SEM, * indicates p < 0.05 and **
 591 indicates p < 0.01 for the comparison of with vs. without added unlabeled lactate.
 592



593

594 **Fig. 6. Lactate can enhance transport of glucose across a monolayer of**
595 **RPE cells. A.** Strategy to evaluate the effect of lactate on transport of glucose
596 across a monolayer of RPE cells. Without lactate (left) glycolysis consumes
597 glucose before it can cross the RPE cell monolayer. With lactate on the apical
598 side (right) glycolysis is partially suppressed so more glucose can cross the
599 monolayer without being consumed by glycolysis. **B.** Lactate (unlabeled) on the
600 apical side enhances transport of U-¹³C glucose (U-¹³C Glc) (measured after 24
601 hours) from the basolateral to apical side of the RPE cell monolayer (n = 3 for
602 each condition; representative of 3 separate experiments, error bars represent
603 StDev * indicates p < 0.05 compared to no added lactate). **C.** Addition of lactate
604 (unlabeled) to the apical side enhances transport of ¹³C Glc from the basolateral
605 side to the apical side (left) (measured after 8 hours) and it suppresses the
606 formation and/or release of ¹³C lactate (right) into the medium on the apical side.
607 (n = 3 for each data point, error bars represent StDev).





631

632

633

634

635

636

637

Fig. 8. A working model that describes the flow of metabolic energy in the retina-RPE ecosystem. Photoreceptors convert glucose into lactate and release the lactate into the interphotoreceptor matrix. Lactate suppresses glycolysis in RPE cells by depleting NAD⁺. Lactate also fuels metabolic activity in Müller cells, which lack key enzymes that would be required for glycolysis.

638

REFERENCES

639

640 1. Bramall AN, Wright AF, Jacobson SG, McInnes RR. The genomic, biochemical,
641 and cellular responses of the retina in inherited photoreceptor degenerations and
642 prospects for the treatment of these disorders. *Annu Rev Neurosci.* 2010;33:441-72.

643

644 2. Punzo C, Kornacker K, Cepko CL. Stimulation of the insulin/mTOR pathway
645 delays cone death in a mouse model of retinitis pigmentosa. *Nat Neurosci.*
2009;12(1):44-52.

646

647 3. Zhang L, Du J, Justus S, Hsu CW, Bonet-Ponce L, Wu WH, et al.
648 Reprogramming metabolism by targeting sirtuin 6 attenuates retinal degeneration. *J Clin
Invest.* 2016;126(12):4659-73.

649

650 4. Sengillo JD, Justus S, Cabral T, Tsang SH. Correction of Monogenic and
Common Retinal Disorders with Gene Therapy. *Genes (Basel).* 2017;8(2).

651

652 5. Du J, Cleghorn W, Contreras L, Linton JD, Chan GC, Chertov AO, et al.
653 Cytosolic reducing power preserves glutamate in retina. *Proc Natl Acad Sci U S A.*
2013;110(46):18501-6.

654

655 6. Du J, Cleghorn WM, Contreras L, Lindsay K, Rountree AM, Chertov AO, et al.
656 Inhibition of mitochondrial pyruvate transport by zaprinast causes massive accumulation
657 of aspartate at the expense of glutamate in the retina. *J Biol Chem.* 2013;288(50):36129-
40.

658

659 7. Du J, Linton JD, Hurley JB. Probing Metabolism in the Intact Retina Using Stable
Isotope Tracers. *Methods Enzymol.* 2015;561:149-70.

660

661 8. Du J, Rountree A, Cleghorn WM, Contreras L, Lindsay KJ, Sadilek M, et al.
662 Phototransduction Influences Metabolic Flux and Nucleotide Metabolism in Mouse
Retina. *J Biol Chem.* 2016;291(9):4698-710.

663

664 9. Du J, Yanagida A, Knight K, Engel AL, Vo AH, Jankowski C, et al. Reductive
665 carboxylation is a major metabolic pathway in the retinal pigment epithelium. *Proc Natl
Acad Sci U S A.* 2016;113(51):14710-5.

666

667 10. Lindsay KJ, Du J, Sloat SR, Contreras L, Linton JD, Turner SJ, et al. Pyruvate
668 kinase and aspartate-glutamate carrier distributions reveal key metabolic links between
neurons and glia in retina. *Proc Natl Acad Sci U S A.* 2014;111(43):15579-84.

669

670 11. Linton JD, Holzhausen LC, Babai N, Song H, Miyagishima KJ, Stearns GW, et al.
671 Flow of energy in the outer retina in darkness and in light. *Proc Natl Acad Sci U S A.*
2010;107(19):8599-604.

672

673 12. Lehmann GL, Benedicto I, Philp NJ, Rodriguez-Boulan E. Plasma membrane
674 protein polarity and trafficking in RPE cells: past, present and future. *Exp Eye Res.*
2014;126:5-15.

675

676 13. Warburg O, Posener, K., Negrelein, E. On the metabolism of carcinoma cells.
Biochemische Zeitschrift. 1924;152:309-44.

- 677 14. Krebs HA. On the metabolism of the retina. *Biochemische Zeitschrift*.
678 1927;189:57-9.
- 679 15. Winkler BS. Glycolytic and oxidative metabolism in relation to retinal function. *J*
680 *Gen Physiol*. 1981;77(6):667-92.
- 681 16. Medrano CJ, Fox DA. Oxygen consumption in the rat outer and inner retina: light-
682 and pharmacologically-induced inhibition. *Exp Eye Res*. 1995;61(3):273-84.
- 683 17. Wang L, Tornquist P, Bill A. Glucose metabolism in pig outer retina in light and
684 darkness. *Acta Physiol Scand*. 1997;160(1):75-81.
- 685 18. Chinchore Y, Begaj, T., Wu, D., Drokhlyansky, E., Cepko, C.L. Glycolytic reliance
686 promotes anabolism in photoreceptors. *bioRxiv*. 2017.
- 687 19. Rajala RV, Rajala A, Kooker C, Wang Y, Anderson RE. The Warburg Effect
688 Mediator Pyruvate Kinase M2 Expression and Regulation in the Retina. *Sci Rep*.
689 2016;6:37727.
- 690 20. Rueda EM, Johnson JE, Jr., Giddabasappa A, Swaroop A, Brooks MJ, Sigel I, et
691 al. The cellular and compartmental profile of mouse retinal glycolysis, tricarboxylic acid
692 cycle, oxidative phosphorylation, and ~P transferring kinases. *Mol Vis*. 2016;22:847-85.
- 693 21. Venkatesh A, Ma S, Le YZ, Hall MN, Ruegg MA, Punzo C. Activated mTORC1
694 promotes long-term cone survival in retinitis pigmentosa mice. *J Clin Invest*.
695 2015;125(4):1446-58.
- 696 22. Kurihara T, Westenskow PD, Gantner ML, Usui Y, Schultz A, Bravo S, et al.
697 Hypoxia-induced metabolic stress in retinal pigment epithelial cells is sufficient to induce
698 photoreceptor degeneration. *Elife*. 2016;5.
- 699 23. Zhao C, Yasumura D, Li X, Matthes M, Lloyd M, Nielsen G, et al. mTOR-
700 mediated dedifferentiation of the retinal pigment epithelium initiates photoreceptor
701 degeneration in mice. *J Clin Invest*. 2011;121(1):369-83.
- 702 24. Gospe SM, 3rd, Baker SA, Arshavsky VY. Facilitative glucose transporter Glut1
703 is actively excluded from rod outer segments. *J Cell Sci*. 2010;123(Pt 21):3639-44.
- 704 25. Badr GA, Tang J, Ismail-Beigi F, Kern TS. Diabetes downregulates GLUT1
705 expression in the retina and its microvessels but not in the cerebral cortex or its
706 microvessels. *Diabetes*. 2000;49(6):1016-21.
- 707 26. Yoshioka K, Takahashi H, Homma T, Saito M, Oh KB, Nemoto Y, et al. A novel
708 fluorescent derivative of glucose applicable to the assessment of glucose uptake activity
709 of *Escherichia coli*. *Biochim Biophys Acta*. 1996;1289(1):5-9.
- 710 27. Giarmarco MM, Cleghorn WM, Sloat SR, Hurley JB, Brockerhoff SE.
711 Mitochondria maintain distinct Ca²⁺ pools in cone photoreceptors. *J Neurosci*. 2017.
- 712 28. Wohl SG, Reh TA. The microRNA expression profile of mouse Muller glia in vivo
713 and in vitro. *Sci Rep*. 2016;6:35423.

- 714 29. Raymond PA, Colvin SM, Jabeen Z, Nagashima M, Barthel LK, Hadidjojo J, et al.
715 Patterning the cone mosaic array in zebrafish retina requires specification of ultraviolet-
716 sensitive cones. *PLoS One*. 2014;9(1):e85325.
- 717 30. Shin J, Chen J, Solnica-Krezel L. Efficient homologous recombination-mediated
718 genome engineering in zebrafish using TALE nucleases. *Development*.
719 2014;141(19):3807-18.
- 720 31. Ablonczy Z, Dahrouj M, Tang PH, Liu Y, Sambamurti K, Marmorstein AD, et al.
721 Human retinal pigment epithelium cells as functional models for the RPE in vivo. *Invest*
722 *Ophthalmol Vis Sci*. 2011;52(12):8614-20.
- 723 32. Adijanto J, Philp NJ. Cultured primary human fetal retinal pigment epithelium
724 (hfRPE) as a model for evaluating RPE metabolism. *Exp Eye Res*. 2014;126:77-84.
- 725 33. Blenkinsop TA, Saini JS, Maminishkis A, Bharti K, Wan Q, Banzon T, et al.
726 Human Adult Retinal Pigment Epithelial Stem Cell-Derived RPE Monolayers Exhibit Key
727 Physiological Characteristics of Native Tissue. *Invest Ophthalmol Vis Sci*.
728 2015;56(12):7085-99.
- 729 34. Johnson LV, Forest DL, Banna CD, Radeke CM, Maloney MA, Hu J, et al. Cell
730 culture model that mimics drusen formation and triggers complement activation
731 associated with age-related macular degeneration. *Proc Natl Acad Sci U S A*.
732 2011;108(45):18277-82.
- 733 35. Sonoda S, Spee C, Barron E, Ryan SJ, Kannan R, Hinton DR. A protocol for the
734 culture and differentiation of highly polarized human retinal pigment epithelial cells. *Nat*
735 *Protoc*. 2009;4(5):662-73.
- 736 36. Metallo CM, Walther JL, Stephanopoulos G. Evaluation of ¹³C isotopic tracers
737 for metabolic flux analysis in mammalian cells. *J Biotechnol*. 2009;144(3):167-74.
- 738 37. Curcio CA, Millican CL, Allen KA, Kalina RE. Aging of the human photoreceptor
739 mosaic: evidence for selective vulnerability of rods in central retina. *Invest Ophthalmol*
740 *Vis Sci*. 1993;34(12):3278-96.
- 741 38. Friedman DS, O'Colmain BJ, Munoz B, Tomany SC, McCarty C, de Jong PT, et
742 al. Prevalence of age-related macular degeneration in the United States. *Arch*
743 *Ophthalmol*. 2004;122(4):564-72.
- 744 39. Casson RJ, Wood JP, Han G, Kittipassorn T, Peet DJ, Chidlow G. M-Type
745 Pyruvate Kinase Isoforms and Lactate Dehydrogenase A in the Mammalian Retina:
746 Metabolic Implications. *Invest Ophthalmol Vis Sci*. 2016;57(1):66-80.
- 747 40. Riepe RE, Norenburg MD. Muller cell localisation of glutamine synthetase in rat
748 retina. *Nature*. 1977;268(5621):654-5.
- 749 41. Hurley JB, Lindsay KJ, Du J. Glucose, lactate, and shuttling of metabolites in
750 vertebrate retinas. *J Neurosci Res*. 2015;93(7):1079-92.

- 751 42. Terluk MR, Kappahn RJ, Soukup LM, Gong H, Gallardo C, Montezuma SR, et
752 al. Investigating mitochondria as a target for treating age-related macular degeneration.
753 J Neurosci. 2015;35(18):7304-11.
- 754 43. Punzo C, Xiong W, Cepko CL. Loss of daylight vision in retinal degeneration: are
755 oxidative stress and metabolic dysregulation to blame? J Biol Chem. 2012;287(3):1642-
756 8.
- 757 44. Ait-Ali N, Fridlich R, Millet-Puel G, Clerin E, Delalande F, Jaillard C, et al. Rod-
758 derived cone viability factor promotes cone survival by stimulating aerobic glycolysis.
759 Cell. 2015;161(4):817-32.
- 760 45. Wang W, Lee SJ, Scott PA, Lu X, Emery D, Liu Y, et al. Two-Step Reactivation
761 of Dormant Cones in Retinitis Pigmentosa. Cell Rep. 2016;15(2):372-85.
- 762 46. Adijanto J, Du J, Moffat C, Seifert EL, Hurley JB, Philp NJ. The retinal pigment
763 epithelium utilizes fatty acids for ketogenesis. J Biol Chem. 2014;289(30):20570-82.
- 764 47. Joyal JS, Sun Y, Gantner ML, Shao Z, Evans LP, Saba N, et al. Retinal lipid and
765 glucose metabolism dictates angiogenesis through the lipid sensor Ffar1. Nat Med.
766 2016;22(4):439-45.
- 767 48. Reyes-Reveles J, Dhingra A, Alexander D, Bragin A, Philp NJ, Boesze-Battaglia
768 K. Phagocytosis Dependent Ketogenesis in Retinal Pigment Epithelium. J Biol Chem.
769 2017.
- 770 49. Akimoto M, Cheng H, Zhu D, Brzezinski JA, Khanna R, Filippova E, et al.
771 Targeting of GFP to newborn rods by Nrl promoter and temporal expression profiling of
772 flow-sorted photoreceptors. Proc Natl Acad Sci U S A. 2006;103(10):3890-5.
- 773 50. Mattapallil MJ, Wawrousek EF, Chan CC, Zhao H, Roychoudhury J, Ferguson
774 TA, et al. The Rd8 mutation of the Crb1 gene is present in vendor lines of C57BL/6N
775 mice and embryonic stem cells, and confounds ocular induced mutant phenotypes.
776 Invest Ophthalmol Vis Sci. 2012;53(6):2921-7.
- 777 51. Wei H, Xun Z, Granado H, Wu A, Handa JT. An easy, rapid method to isolate
778 RPE cell protein from the mouse eye. Exp Eye Res. 2016;145:450-5.
- 779 52. Collymore C, Rasmussen S, Tolwani RJ. Gavaging adult zebrafish. J Vis Exp.
780 2013(78).
- 781 53. Uhlen M, Fagerberg L, Hallstrom BM, Lindskog C, Oksvold P, Mardinoglu A, et al.
782 Proteomics. Tissue-based map of the human proteome. Science.
783 2015;347(6220):1260419.
784